

The fate of phonons in freely expanding Bose-Einstein condensates

C. Tozzo

Dipartimento di Fisica, Università di Trento, and Istituto Nazionale per la Fisica della Materia, BEC-INFM Trento, I-38050 Povo, Italy

F. Dalfovo

Dipartimento di Matematica e Fisica, Università Cattolica, Via Musei 41, 25121 Brescia and Istituto Nazionale per la Fisica della Materia, Unità di Brescia and BEC-INFM Trento

(Dated: July 9, 2018)

Phonon-like excitations can be imprinted into a trapped Bose-Einstein condensate of cold atoms using light scattering. If the condensate is suddenly let to freely expand, the initial phonons lose their collective character by transferring their energy and momentum to the motion of individual atoms. The basic mechanisms of this evaporation process are investigated by using the Gross-Pitaevskii theory and dynamically rescaled Bogoliubov equations. Different regimes of evaporation are shown to occur depending on the phonon wavelength. Distinctive signatures of the evaporated phonons are visible in the density distribution of the expanded gas, thus providing a new type of spectroscopy of Bogoliubov excitations.

PACS numbers: 03.75 Fi

I. INTRODUCTION

Bose-Einstein condensates of cold atoms represent a remarkable testing ground for theories of weakly interacting bosons. The fact that the actual condensates are spatially confined and inhomogeneous makes these systems even more interesting. From one hand, the Bogoliubov theory of uniform gases [1] can still be applied in certain limits, when the system can be viewed as “locally uniform”. Such a local density approach has been used, for instance, to characterize the response of a condensate to light scattering processes [2, 3, 4, 5, 6, 7, 8]. In the same spirit, properties of the uniform gas can also be extracted from a trapped condensate by reducing the effects of inhomogeneous broadening as suggested in Ref. [9]. On the other hand, finite size effects are interesting by themselves, giving rise to a new type of Bogoliubov excitations with spatially varying quasiparticle amplitudes, such as the low frequency collective oscillations of the whole condensate (see [10] and references therein) and the axial phonons of elongated condensates, exhibiting a multibranch spectrum [11, 12].

In most of the experiments with excited condensates, the observations are performed after switching-off the confining potential and letting the condensate to expand. The comparison between theory and experimental data often ignores the dynamics of the expansion. This is justified if one looks for quantities that are conserved during the expansion like, for instance, the total momentum of the condensate. However, the expansion of a condensate initially dressed with phonon-like modes is interesting from both the conceptual and experimental viewpoints. Conceptually, the behavior of an excited state that starts as a quasiparticle and evolves into a particle is a remarkable and nontrivial example of quantum process, which shows some similarities with the quantum evaporation process at the surface of superfluid helium [13] and with the evolution of two-level systems with nonhermitian Hamiltonian [14]. From the experimental viewpoint, on the other hand, the characterization of the observable density and velocity distri-

butions of the expanded gas in terms of specific initial configurations is important in order to use those distributions as a probe of in-trap quasiparticles.

In this paper we use the Gross-Pitaevskii (GP) theory to investigate the expansion of elongated axially symmetric condensates. We assume the initial configuration to be a stationary trapped condensate at zero temperature. The condensate is excited by populating some quasiparticle states and, then, let to expand.

In section II, we first present the results of numerical simulations based on the direct integration of the time dependent Gross-Pitaevskii equation in the case of an elongated condensate similar to the one of recent experiments [4, 5, 11]. We show that the expansion exhibits quite different behaviors depending on the wavelength of the initial phonons: i) long wavelength phonons remain inside the expanding condensate in the form of density modulations; ii) short wavelength phonons are converted into a separate cloud of excited atoms moving out of the condensate. In both cases, the final density distribution shows nontrivial features, such as a radial distortion of the density modulations in the condensate and a “shell” structure of the released-phonon cloud.

In section III, we use the simplified geometry of an infinite cylindrical condensate in order to get a deeper insight, pointing out the different role of radial and axial degrees of freedom. In this case, we numerically solve the Bogoliubov equations for the amplitudes of in-trap quasiparticles. Then we follow the expansion of a condensate initially dressed with one of these quasiparticles by using the scaling properties of the GP equation in two-dimensions and solving rescaled Bogoliubov-like equations. This approach allows us to characterize the behavior of the excitations during the expansion, at different levels of approximation, and to find the relevant timescales for the evaporation process. Interesting results can also be obtained by averaging out the slow radial motion of the excitations in the rescaled coordinates. The problem is thus mapped into the evolution of a quasiparticle in a uniform gas with a decreasing time-dependent density. In section IV,

we show that this process can be either adiabatic (conversion of a quasiparticle into a single particle with the same momentum) or non-adiabatic depending on the phonon wavelength and on the chemical potential of the gas.

In section V, we compare the predictions of the rescaled Bogoliubov equations for the infinite cylinder with the results of GP simulations for elongated condensates. The comparison is instructive and allows one to relate the properties of in-trap quasiparticles with observable features of the expanded gas. In particular, we discuss the axial motion of density modulations, the radial scaling of nodal lines, the conditions for the appearance of a separate released-phonon cloud and for the adiabaticity of the quasiparticle evaporation process.

The expansion of condensates with long wavelength phonons was previously studied in Ref. [15], where random phase fluctuations were included in the configuration of a very elongated condensate at the beginning of the expansion, in order to simulate the behavior of a quasi-condensate with thermal excitations. Low energy phonons that expand in the hydrodynamic regime were also considered in [16] as due to “quantum vacuum” phase fluctuations. Instead of investigating the effects of thermal and/or quantum fluctuations, we are here considering situations where the initial excitations are imprinted in a controllable way and characterized by looking at the shape of the expanded gas, thus allowing for a new type of spectroscopic studies of Bogoliubov quasiparticles.

II. GP NUMERICAL SIMULATIONS FOR ELONGATED CONDENSATES

We simulate a process of quasiparticle creation and expansion in a realistic axially symmetric, cigar-shaped, condensate. The starting point is the time dependent GP equation for the order parameter $\Psi(x, y, z, t)$ of a condensate of N bosonic atoms of mass m [10, 17]:

$$i\hbar\partial_t\Psi = \left(-\frac{\hbar^2\nabla^2}{2m} + V + gN|\Psi|^2 \right) \Psi, \quad (1)$$

where $g = 4\pi\hbar^2 a/m$, and a is the s -wave scattering length that we assume to be positive. The order parameter is here normalized according to $\int d\mathbf{r}|\Psi|^2 = 1$.

Let us first take the harmonic trapping potential in the form

$$V(\rho, z) = V_{\text{trap}}(\rho, z) = (1/2)m\omega_\rho^2(\rho^2 + \lambda^2 z^2) \quad (2)$$

where $\rho = [x^2 + y^2]^{1/2}$ and $\lambda = \omega_z/\omega_\rho$. The ground state can be found as the stationary solution of Eq. (1). In practice we map the order parameter on a $N_\rho \times N_z$ grid (typically, 64×1024 points) and propagate it in imaginary time with an explicit first order algorithm starting from a trial configuration, as described in Ref. [18]. If $\lambda < 1$ the condensate at equilibrium is a prolate ellipsoid.

Excitations can be created in the condensate by using light (Bragg) scattering [2, 3, 4, 5, 6]. Within the GP theory, this is accounted for by adding an extra term to the external potential,

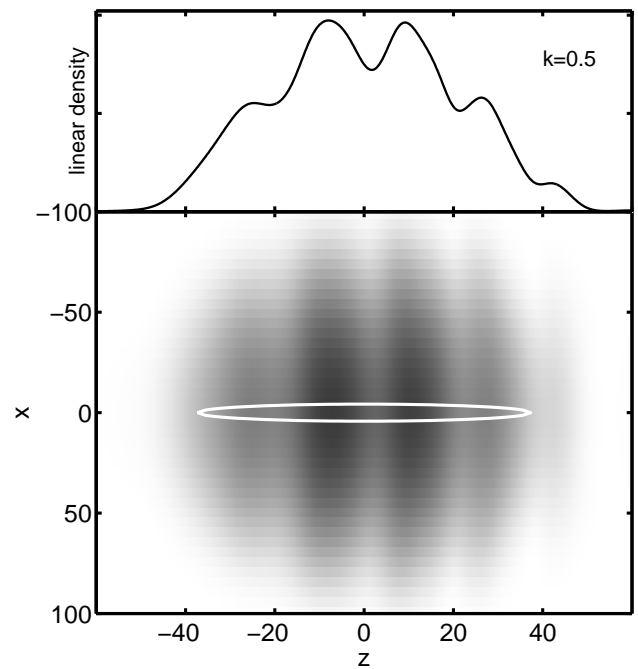


FIG. 1: Column (below) and linear (above) density, in arbitrary units, of a condensate subject to a Bragg pulse with $k = 0.5a_\rho^{-1}$, $\omega = 1.1\omega_\rho$, $V_B = 0.2\hbar\omega_\rho$ and $t_B = 4\omega_\rho^{-1}$, and a subsequent free expansion of $t = 25\omega_\rho^{-1}$. The white ellipse is the shape of the condensate at $t = 0$, at the beginning of the expansion. Distances are in units of $a_\rho = [\hbar/(m\omega_\rho)]^{1/2}$.

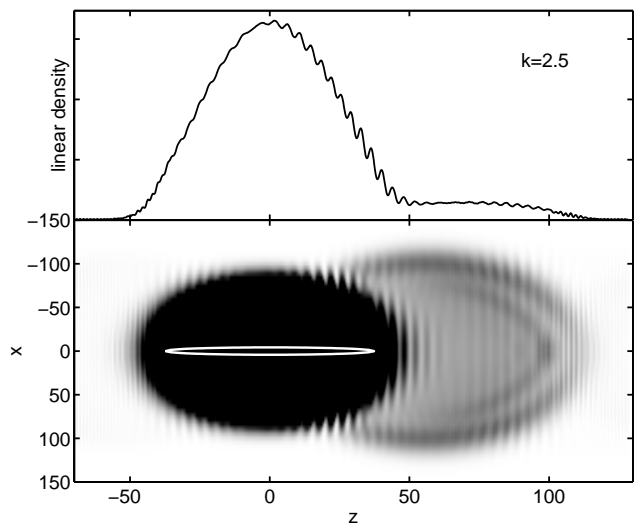


FIG. 2: Same as before, but for a Bragg pulse with $k = 2.5a_\rho^{-1}$, $\omega = 4.7\omega_\rho$, $V_B = 1\hbar\omega_\rho$ and $t_B = 1\omega_\rho^{-1}$.

that becomes [19]

$$V(\rho, z, t) = V_{\text{trap}}(\rho, z) + V_B \cos(kz - \omega t) \quad (3)$$

for $-t_B < t < 0$ and assuming the momentum transfer to be along z . We numerically integrate the GP equation (1) by propagating the order parameter in real time, starting from the

ground state configuration at $t = -t_B$. We split the propagation into the axial and radial parts. The former is obtained by using a fast Fourier transform algorithm to treat the kinetic energy term, while the latter is performed with a Crank-Nicholson differencing method, as in Refs. [8, 11, 12].

Now, let's suppose that both the Bragg pulse and the external trapping potential are switched-off at $t = 0$. The condensate freely expands and the expansion can still be studied by solving the GP equation. We use the same algorithm as before with the only difference that we rescale all distances during the expansion in order to keep the box size and the number of grid points the same as for the trapped condensate. For that we use a dynamically rescaled GP equation already introduced in [20, 21].

For our simulations we choose the parameters of the condensate used in the experiments of Nir Davidson and co-workers [4, 5, 6, 11], made of $N = 10^5$ atoms of ^{87}Rb in a trap with $\omega_\rho = 2\pi(220\text{Hz})$ and $\lambda = 0.114$. We plot distances in units of the harmonic oscillator length $a_\rho = [\hbar/(m\omega_\rho)]^{1/2}$, time in units of ω_ρ^{-1} and energies in units of $\hbar\omega_\rho$. The chemical potential is $\mu = 9.1\hbar\omega_\rho$. Several condensates in current experiments have similar parameters.

Typical results are shown in Figs. 1 and 2, where we plot the column density, $\int dy |\Psi(x, y, z)|^2$, and the linear density, $\int dx dy |\Psi(x, y, z)|^2$, for two sets of parameters of the Bragg pulse. The values are chosen such that the lowest longitudinal modes are resonantly excited. Moreover, both values of k are smaller than $\xi^{-1} \simeq 3a_\rho^{-1}$, where ξ is the healing length. This implies that in both cases the excitations are collective phonon-like Bogoliubov quasiparticles.

There is a dramatic difference between the density distributions for the two values of k . At low k all atoms remain within the expanding condensate that exhibits an evident density modulation, while at high k an extra cloud of excited atoms separates out in the positive z direction.

In order to get a better view of the behavior of expanding phonons one can repeat each simulation twice for the same condensate with and without excitations (Bragg pulse "on" and "off") and calculate the density difference $\Delta n(\rho, z) = N[|\Psi_{\text{on}}(x, y, z)|^2 - |\Psi_{\text{off}}(x, y, z)|^2]$. When the number of quasiparticles is much smaller than N , this quantity converges to the density variation, $\delta n(\rho, z)$, associated with the excitations in the linear response regime. In Figs. 3 and 4 we show the results for the two sets of parameters of Figs. 1 and 2, respectively.

At $k = 0.5a_\rho^{-1}$ we observe well defined wavefronts. They reflect the density modulations associated with the initial phonon at $t = 0$ (dashed line in the upper plot). These modulations move along z during the expansion. Their velocity depends on both z and ρ and is faster for $\rho = 0$, where the density is higher. This causes each front to be slightly bent. Effects of such a bending are also visible in Fig. 1 in the form of a small asymmetry of the modulations of both the column and linear densities. In Fig. 5 we show the position $z(t)$ of a wavefront for $\rho = 0, 0.4$ and $0.8R$ (points A, B and C in Fig. 3), where R is radial size of the expanding condensate. The initial velocity is very close to the sound velocity in a cylindrical condensate, $c = [gn(0)/(2m)]^{1/2}$ [22], having the

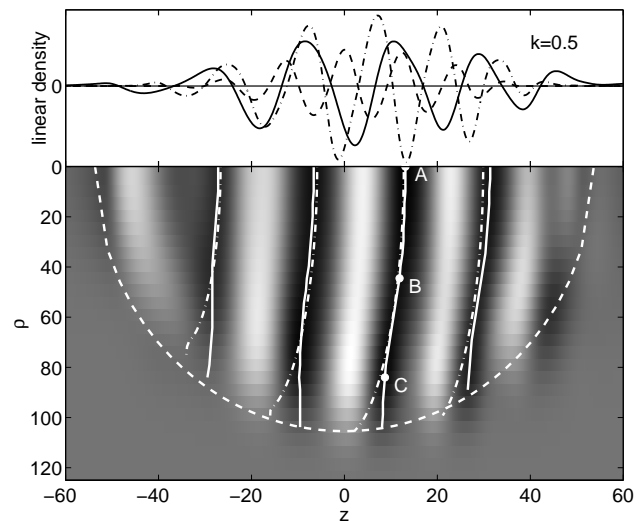


FIG. 3: Lower part: the quantity $\Delta n(\rho, z)$ at $t = 25\omega_\rho^{-1}$ is plotted, in arbitrary units, for the same simulation of Fig. 1. Black (white) means positive (negative) $\Delta n(\rho, z)$. The dashed line is the position of the surface of the expanding condensate. The uniform grey colour far outside the condensate corresponds to $\Delta n = 0$. Solid lines are the position of maxima of $\Delta n(\rho, z)$ (wavefronts). Dot-dashed lines are the same wavefronts estimated by means of Eq. (49). Upper part: integrated density variation $2\pi \int d\rho \rho \Delta n$, calculated at $t = 0$ (dashed), 10 (dot-dashed) and $25\omega_\rho^{-1}$ (solid).

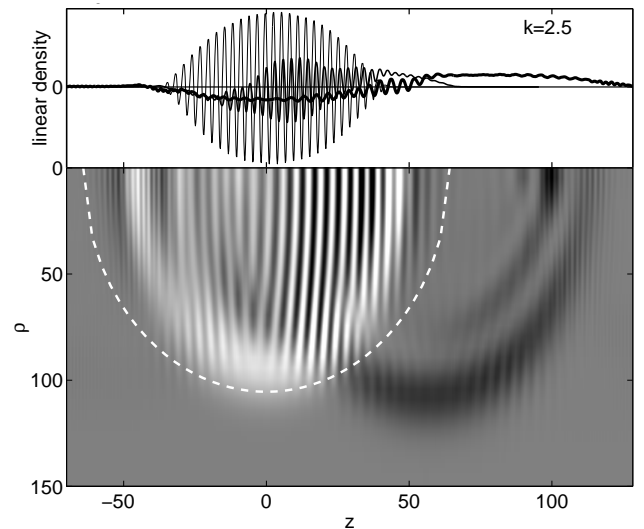


FIG. 4: Lower part: the quantity $\Delta n(\rho, z)$ at $t = 25\omega_\rho^{-1}$ is plotted, in arbitrary units, for the same simulation of Fig. 2. The meaning of the greyscale is the same as in the lower part of Fig. 3. Upper part: integrated density variation $2\pi \int d\rho \rho \Delta n$, calculated at $t = 0, 10$ and $25\omega_\rho^{-1}$ from thin to thick solid line, respectively.

same density profile $n(\rho)$ at $z = 0$.

At $k = 2.5a_\rho^{-1}$ the main feature is the shape of the cloud of excited atoms that are moving out of the condensate. By using the order parameter $\Psi(x, y, z)$, one can calculate the local contribution to the total energy and momentum of the system. Most of the energy of the condensate is, of course, in the ki-

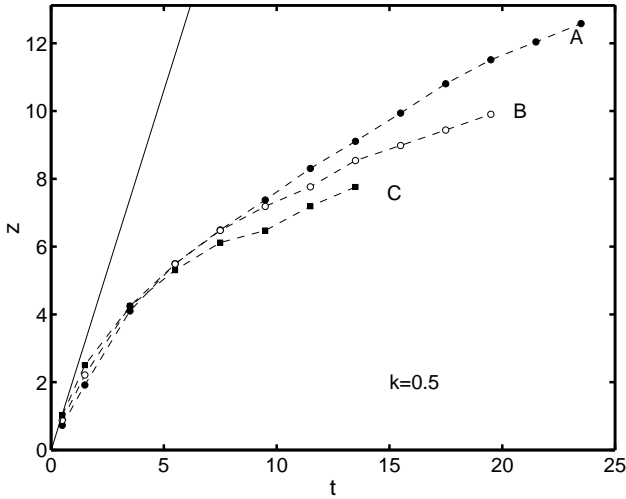


FIG. 5: Position $z(t)$ of a wavefront for $k = 0.5a_\rho^{-1}$ and $\rho = 0, 0.4$ and $0.8R$ (points A, B and C in Fig. 3), where R is the radial size of the expanding condensate. The thin solid line is $z(t) = ct$, where $c = [gn(0)/(2m)]^{1/2}$ is the sound velocity in a cylindrical condensate with the same central density $n(0)$.

netic energy of the fast radial motion. What is more important, however, is that the initial excitation energy, i.e., the energy of the excited phonons, is almost completely transferred to the lateral cloud, which is moving along z at a velocity of the order of $\hbar k/m$. The shape of this cloud exhibits an interesting “shell” structure with some lobes divided by almost empty regions. The appearance of this extra cloud is accompanied by a strong suppression of density modulations in the condensate.

By performing several simulations at different k we find a transition from the low- k scenario (density modulations within the expanding condensate) and the higher k scenario (external cloud of atoms) occurring in between $k = 0.5$ and $1a_\rho^{-1}$. The experiments so far performed with phonons excited by Bragg scattering [2, 3, 4, 5, 6, 11] belongs to the second scenario. Using a tomographic imaging method the authors of Ref. [5] found that the observed released-phonon cloud has indeed a nontrivial shell-like shape. First evidences of the first scenario have also been found in recent experiments of the same group [23], where density modulations have been observed at low k within the condensate. Before coming back to the interpretation of our GP simulations, let us explore the instructive case of an infinite cylindrical condensate.

III. BOGOLIUBOV EXCITATIONS IN EXPANDING CYLINDRICAL CONDENSATES

A. Bogoliubov excitations in trap

Here we consider a condensate that is unbound along z and radially confined in the harmonic potential $V(\rho) = (1/2)m\omega_\rho^2\rho^2$. In this geometry one can better distinguish the different roles played by radial and axial degrees of freedom. The order parameter of the ground state only depends on ρ

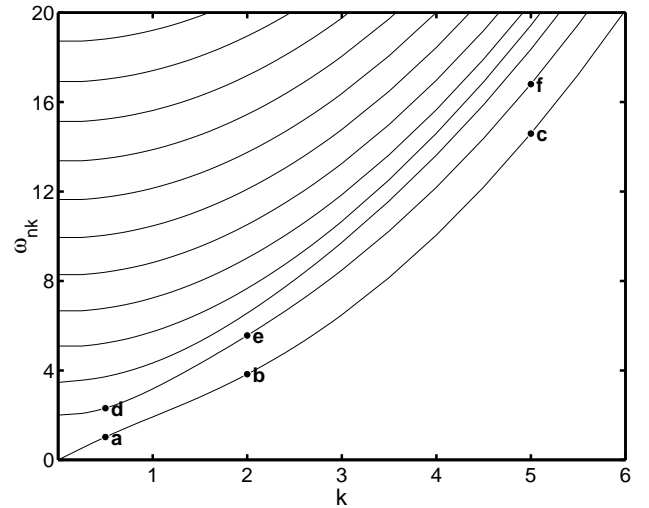


FIG. 6: Spectrum of axially symmetric Bogoliubov excitations of a cylindrical condensate with $\eta = 9.1$. The frequency ω_{nk} , in units of the radial trapping frequency ω_ρ , is plotted as a function of the axial wavevector k , in units of a_ρ^{-1} . The number of radial nodes is $n = 0, 1, 2, \dots$, starting from the lowest branch. The quasiparticle amplitudes u and v of the modes a, b, c, d, e and f are shown in the first column of Figs. 7 and 8.

and obeys the stationary GP equation

$$\left[-\frac{\hbar^2 \nabla_\rho^2}{2m} + V(\rho) + gn_0(\rho) \right] \Psi_0(\rho) = \mu \Psi_0(\rho) \quad (4)$$

where μ is the chemical potential and Ψ_0 is chosen to be real and subject to the normalization condition $2\pi \int_0^\infty d\rho \rho \Psi_0^2 = 1$, so that $n_0(\rho) = (N/L)\Psi_0^2(\rho)$ is the ground state density. The excited states are plane waves along z , with wavevector k . Different branches of such longitudinal waves exist, characterized by the number of nodes in the radial direction, n . When the condensate is weakly excited in one of these modes, its order parameter can be written as

$$\Psi(\rho, z, t) = e^{-i\mu t/\hbar} [\Psi_0(\rho) + \delta\Psi(\rho, z, t)] \quad (5)$$

where

$$\delta\Psi(\rho, z, t) = L^{-1/2} \left[u_{nk}(\rho) e^{i(kz - \omega_{nk}t)} + v_{nk}^*(\rho) e^{-i(kz - \omega_{nk}t)} \right]. \quad (6)$$

Inserting this expression into Eq. (1) one gets the Bogoliubov equation

$$\begin{pmatrix} H_\rho + \frac{\hbar^2 k^2}{2m} & gn_0(\rho) \\ -gn_0(\rho) & -H_\rho - \frac{\hbar^2 k^2}{2m} \end{pmatrix} \begin{pmatrix} u_{nk} \\ v_{nk} \end{pmatrix} = \hbar\omega_{nk} \begin{pmatrix} u_{nk} \\ v_{nk} \end{pmatrix} \quad (7)$$

where

$$H_\rho = -\frac{\hbar^2 \nabla_\rho^2}{2m} + V(\rho) + 2gn_0(\rho) - \mu. \quad (8)$$

The quasiparticle amplitudes u_{nk} and v_{nk} obey the following orthogonality and symmetry relations

$$\int d\rho 2\pi\rho(u_{nk}u_{n'k'}^* - v_{nk}v_{n'k'}^*) = \delta_{nn'}\delta(k - k') \quad (9)$$

$$\int d\rho \rho(u_{nk}v_{n'k'} - v_{nk}u_{n'k'}) = 0. \quad (10)$$

Equations (4) and (7) can be solved numerically to get Ψ_0 , u_{nk} , v_{nk} and ω_{nk} [12, 24, 25, 26].

In Fig. 6 we show the spectrum of axial phonons in a cylindrical condensate which simulates the behavior of the elongated condensate discussed in section II. The relevant parameter that characterizes the solutions of the above equations is $\eta \equiv \mu_{\text{TF}}/(\hbar\omega_\rho) = [4aN/L]^{1/2}$, where μ_{TF} is the chemical potential in the Thomas-Fermi limit. The condensate in Fig. 6

has $\eta = 9.1$. Similar spectra were already discussed in details in Ref. [12]. The form of the quasiparticle amplitudes $u_{nk}(\rho)$ and $v_{nk}(\rho)$ for some states on the first two branches is shown in Figs. 7 and 8 ($t = 0$ plots, first column). The modes on the lowest branch have no nodes in the radial direction; those in the first branch have one node, and so on. One also notes that the excited states have a nonvanishing amplitude in the center of the condensate only at low k , while at higher k they are mainly located in the low density region near the surface [10, 27]. Finally, we observe that, as expected, the amplitude v is of the same order of u in the phononic regime at small k , while it is negligible when k is larger than ξ^{-1} . In our case $\xi^{-1} = \eta^{1/2}a_\rho^{-1} \simeq 3a_\rho^{-1}$.

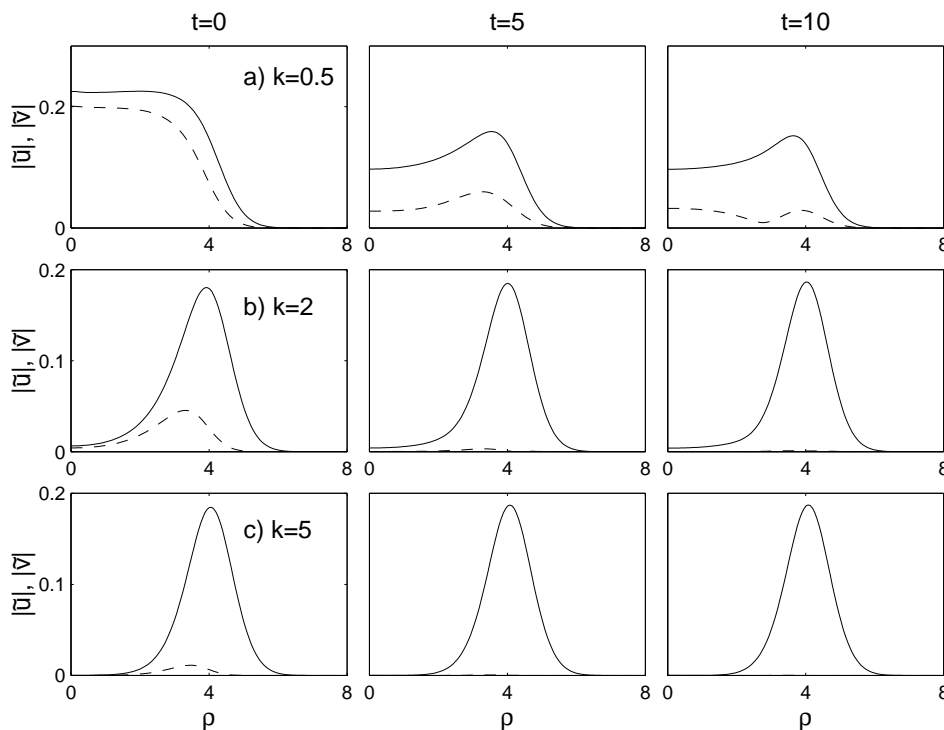


FIG. 7: Time evolution of the functions $|\tilde{u}(\rho)|$ (solid lines) and $|\tilde{v}(\rho)|$ (dashed lines) obtained from Eq. (18). At $t = 0$ these functions coincide with the Bogoliubov amplitudes u_{0k} and v_{0k} , solutions of Eq. (7) for the modes (a), (b), and (c) in the spectrum of Fig. 6. The radial coordinate ρ is given in units of a_ρ . The Thomas-Fermi radius of the condensate is $R = 4.27a_\rho$.

B. Free expansion and scaling

Now let us suppose that the trapping potential is switched-off at $t = 0$. One can introduce a rescaled order parameter $\tilde{\Psi}$ as [28]

$$\Psi(\rho, z, t) = \frac{1}{b(t)} \tilde{\Psi}\left(\frac{\rho}{b(t)}, z, t\right) \exp\left[\frac{im\rho^2\dot{b}(t)}{2\hbar b(t)} - \frac{i\mu\tau(t)}{\hbar}\right] \quad (11)$$

where τ is defined as $\tau(t) = \int_0^t dt'/b^2(t')$. The scaling parameter $b(t)$ obeys the equation

$$\ddot{b}(t) = \omega_\rho^2/b^3(t), \quad (12)$$

with $b(0) = 1$ and $\dot{b}(0) = 0$, whose solution is

$$b(t) = [1 + \omega_\rho^2 t^2]^{1/2}. \quad (13)$$

With this choice, the GP equation (1) for the rescaled order parameter $\tilde{\Psi}(\rho, z, t)$ becomes

$$i\hbar\partial_t\tilde{\Psi} = \frac{1}{b^2(t)} \left(-\frac{\hbar^2\nabla_\rho^2}{2m} + V + \frac{gN}{L}|\tilde{\Psi}|^2 - \mu \right) \tilde{\Psi} - \frac{\hbar^2}{2m} \frac{\partial^2}{\partial z^2} \tilde{\Psi}. \quad (14)$$

A major property of this equation is that, if the rescaled order parameter at $t = 0$ coincides with the t - and z -independent solution of the stationary GP equation (4), then it remains t - and z -independent solution of the same equation forever. Let us call $\tilde{\Psi}_0(\rho)$ this stationary solution. The time evolution of

true order parameter Ψ is entirely accounted for by the scaling parameter $b(t)$ given in (13). The stationary $\tilde{\Psi}_0(\rho)$ thus corresponds to an expanding order parameter with constant shape in the rescaled co-ordinate $\rho/b(t)$ and with a density that decreases in time as $n(\rho, t) = (N/L)\Psi_0^2(\rho/b(t))/b^2(t)$. This behavior is a particular case of a more general scaling property of the GP equation, which is exact in a two-dimensional geometry and is valid for a generic time-dependent trapping frequency $\omega_\rho(t)$ [28, 29, 30]. Here we want to apply Eq. (14) to describe also an expanding condensate whose initial configuration, at $t = 0$, is a superposition of the ground state and some excited states.

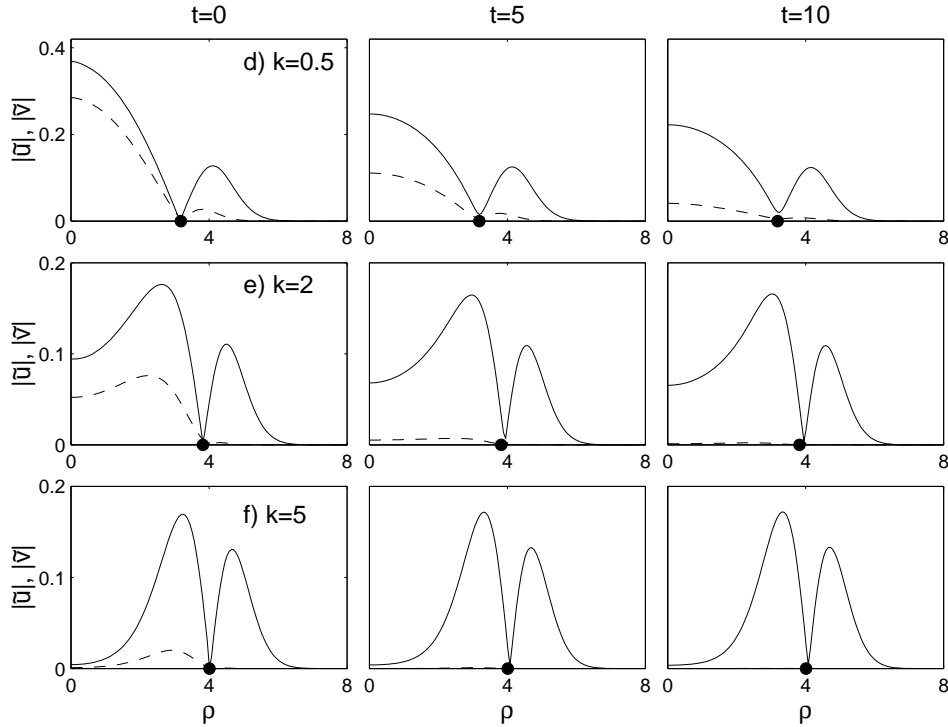


FIG. 8: Same as in Fig. 7, but for the modes (d), (e) and (f). At $t = 0$ the functions $|\tilde{u}|$ and $|\tilde{v}|$ coincide with the Bogoliubov amplitudes u_{1k} and v_{1k} , solutions of Eq. (7) with one radial node. The position of the $t = 0$ node is shown as a black dot on the horizontal axis.

C. Rescaled Bogoliubov-like equations

Let us take the rescaled order parameter in the form $\tilde{\Psi}(\rho, z, t) = \tilde{\Psi}_0(\rho) + \delta\tilde{\Psi}(\rho, z, t)$, where $\tilde{\Psi}_0$ is the (real) solution of the stationary GP equation and $\tilde{n}_0(\rho) = (N/L)\tilde{\Psi}_0^2(\rho)$ is the rescaled density. The linearized version of Eq. (14) is

$$i\hbar\partial_t\delta\tilde{\Psi}(\rho, z, t) = \left[\frac{\tilde{H}_\rho}{b^2(t)} - \frac{\hbar^2\partial_z^2}{2m} \right] \delta\tilde{\Psi}(\rho, z, t) + \frac{g\tilde{n}_0(\rho)}{b^2(t)}\delta\tilde{\Psi}^*(\rho, z, t), \quad (15)$$

with

$$\tilde{H}_\rho = -\frac{\hbar^2\nabla_\rho^2}{2m} + V(\rho) + 2g\tilde{n}_0(\rho) - \mu. \quad (16)$$

Now let us write $\delta\tilde{\Psi}$ in the form

$$\delta\tilde{\Psi}(\rho, z, t) = L^{-1/2}[\tilde{u}(\rho, t)e^{ikz} + \tilde{v}^*(\rho, t)e^{-ikz}]. \quad (17)$$

Inserting this expression into Eq. (15) one gets the following equations for new amplitudes \tilde{u} and \tilde{v}

$$i\hbar\partial_t \begin{pmatrix} \tilde{u} \\ \tilde{v} \end{pmatrix} = \left[\frac{1}{b^2(t)}\mathcal{L}_\rho + \mathcal{L}_z \right] \begin{pmatrix} \tilde{u} \\ \tilde{v} \end{pmatrix} \quad (18)$$

where

$$\mathcal{L}_\rho = \begin{pmatrix} \tilde{H}_\rho & g\tilde{n}_0 \\ -g\tilde{n}_0 & -\tilde{H}_\rho \end{pmatrix}; \quad \mathcal{L}_z = \frac{\hbar^2 k^2}{2m} \begin{pmatrix} 1 & 0 \\ 0 & -1 \end{pmatrix}. \quad (19)$$

These equations describe the behavior of small deviations from the stationary rescaled order parameter $\tilde{\Psi}_0$. At $t < 0$, when $b(t) = 1$ and $\tilde{\Psi} = \Psi$, the t - and ρ -dependence of \tilde{u} and \tilde{v} can be factorized as in Eq. (6) and the rescaled Bogoliubov-like equation (18) reduces to the Bogoliubov equation (7) for the excitations of the trapped condensate. One can select one of these excitations, with given k and n , as initial values of \tilde{u} and \tilde{v} and then solve numerically Eq. (18) for the free expansion at $t > 0$. Typical examples are given in Figs. 7 and 8, where we show the time evolution of $|\tilde{u}(\rho)|$ and $|\tilde{v}(\rho)|$ for six different excited states.

During the expansion \tilde{u} and \tilde{v} exhibit different behaviors: \tilde{u} decreases in time at low k , while it remains almost constant at large k ; vice-versa, \tilde{v} always decreases, but it decreases faster at high k . Let us define the normalized radial average $\langle |\tilde{v}|^2 \rangle = \int d\rho \rho |\tilde{v}(\rho, t)|^2 / \int d\rho \rho |v(\rho, 0)|^2$. In Fig. 9 we plot $\langle |\tilde{v}|^2 \rangle$ as a function of t for different k (solid lines). At large k , all curves approach an universal behavior: \tilde{v} decreases in the typical timescale of the expansion, ω_ρ^{-1} , which is the time needed for the mean-field energy to vanish. Conversely, at low k it decreases much more slowly, approaching a finite value for $t \rightarrow \infty$. This is also evident in Figs. 7 and 8, where the function $|\tilde{v}|$ for the lowest value of k remains well visible also at $t = 5$ and $t = 10\omega_\rho^{-1}$, when the mean-field interaction is certainly negligible. In this regime, the functions \tilde{u} and \tilde{v} have completely lost their initial meaning of quasiparticle amplitudes of Bogoliubov modes; they are simply the two Fourier components of a density and velocity modulation in the expanding ‘‘ideal’’ gas.

From the knowledge of \tilde{u} and \tilde{v} one can also write the rescaled density variation $\delta\tilde{n}$, which is given by

$$\delta\tilde{n} = \tilde{\Psi}_0 |\tilde{u} + \tilde{v}| \cos[kz + \text{phase}(\tilde{u} + \tilde{v})], \quad (20)$$

while $(\tilde{u} - \tilde{v})$ is related to the axial current density. The initial phase can be chosen in such a way that the excitation at $t = 0$ is just a sinusoidal wave of wavelength $2\pi/k$, which moves along z with phase velocity ω_{nk}/k . Then one can look at the time evolution of nodal lines or crests. Typical results are shown in Fig. 10. The results at $k = 0.5a_\rho^{-1}$ can be compared with those obtained from the GP simulations in the elongated condensate for the same k , given in Fig. 5. The qualitative agreement between the two calculations is noticeable, especially if one keeps in mind that the results of Fig. 10 completely ignore the inhomogeneity and finite axial size of the elongated condensate of Fig. 5. The $k = 2a_\rho^{-1}$ case is also interesting, because it shows that the velocity of the fronts quickly approaches the phase velocity of free particles $\hbar k/(2m)$. Finally, from this results it is also clear that the observation of wavefronts, with their phase and amplitude, gives access to the quantity $|\tilde{u} + \tilde{v}|$, while the total momentum transferred is a measure of $(|\tilde{u}|^2 - |\tilde{v}|^2)$ [12]. It is worth noticing that Eq. (18) conserves the total momentum, which is proportional to $\int d\rho \rho (|\tilde{u}|^2 - |\tilde{v}|^2)$.

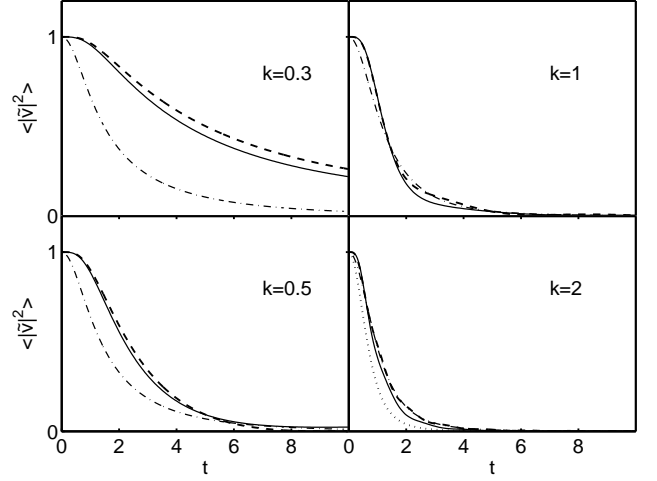


FIG. 9: Normalized radial average of $|\tilde{v}|^2$ as a function of t , in units of ω_ρ^{-1} , for different values of k , in units of a_ρ^{-1} . Solid lines are the results obtained from Eq. (18) for the infinite cylinder. Dashed lines are the results obtained from Eq. (23) or, equivalently, from Eq. (48) and correspond to the behavior of $|\tilde{v}|^2$ in a uniform gas whose density is equal to the radial average of the density of the expanding infinite cylinder. Dot-dashed lines correspond to the adiabatic following approximation (45). For larger values of k all curves converge to the analytic result (46) shown as a dotted line in the bottom-right quadrant.

D. Radial motion: scaling of nodal lines

Now we consider in more details the time evolution of the radial shape of \tilde{u} and \tilde{v} . In the two opposite limits $k = 0$ and $k \rightarrow \infty$ they obey an exact scaling law. Let us consider first the case $k = 0$, i.e., purely radial excitations with an arbitrary number of radial nodes. The quantities \tilde{u} and \tilde{v} are z -independent and Eq. (18) becomes

$$i\hbar\partial_t \begin{pmatrix} \tilde{u} \\ \tilde{v} \end{pmatrix} = \frac{1}{b^2(t)} \mathcal{L}_\rho \begin{pmatrix} \tilde{u} \\ \tilde{v} \end{pmatrix}. \quad (21)$$

As initial condition at $t = 0$, one can choose $\tilde{u}(\rho, 0) = u_{n0}(\rho)$ and $\tilde{v}(\rho, 0) = v_{n0}(\rho)$, where u_{n0} and v_{n0} are the eigenfunctions of the operator \mathcal{L}_ρ with eigenvalues $\hbar\omega_{n0}$, i.e., the $k = 0$ solutions of the Bogoliubov eigenvalue problem (7). Then an exact solution of Eq. (21) is found in the form $\tilde{u}(\rho, t) = \alpha(t)u_{n0}(\rho)$ and $\tilde{v}(\rho, t) = \alpha(t)v_{n0}(\rho)$, with $\alpha(0) = 1$. One finds

$$ib^2(t)\partial_t\alpha(t) = \omega_{n0}\alpha(t), \quad (22)$$

whose solution is $\alpha(t) = \exp[-i\omega_{n0}\tau(t)]$ with $\tau(t) = \int_0^t dt' / [1 + \omega_\rho^2 t'^2] = \omega_\rho^{-1} \text{atan}(\omega_\rho t)$. The phase of \tilde{u} and \tilde{v} has a nontrivial t -dependence, corresponding to a true oscillation of the type $\exp(i\omega_{n0}t)$ only for a short time interval, shorter than the typical expansion time ω_ρ^{-1} , while for longer times the oscillations are frozen. However, the modulus $|\tilde{u}|$ and $|\tilde{v}|$ remains stationary at all times and the radial nodes of these functions remain fixed. This means that the density variation δn has nodes that expand radially with the same scaling law of the whole condensate, governed by $b(t)$.

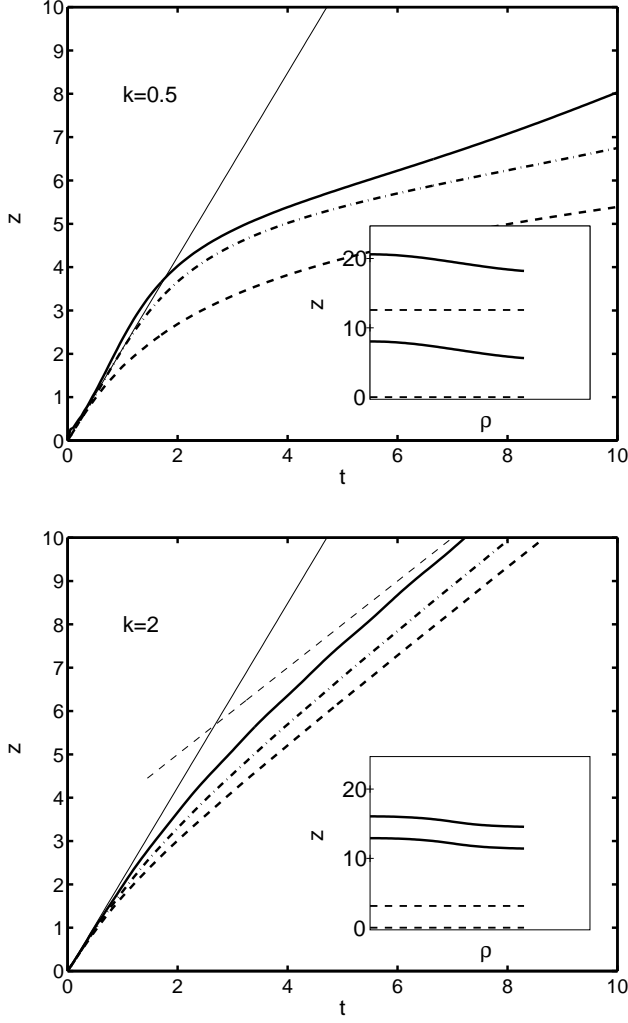


FIG. 10: Wavefront position vs. time for $k = 0.5a_\rho^{-1}$ and $k = 2a_\rho^{-1}$, obtained from the maxima of $\delta\tilde{n}$ defined in Eq. (20) with \tilde{u} and \tilde{v} given by Eq. (18). As in Fig. 5, the wavefront position is plotted for $\rho = 0$ (solid), 0.4 (dot-dashed) and $0.8R$ (dashed), where R is the Thomas-Fermi radius of the condensate. The slope of the thin solid and dashed lines is the Bogoliubov sound velocity, $c = [gn(0)/(2m)]^{1/2}$ and the phase velocity of free particles, $\hbar k/(2m)$, respectively. The inset shows the shape of two nearest fronts at $t = 0$ (dashed lines) and $t = 10\omega_\rho^{-1}$ (solid lines). Each front is plotted from $\rho = 0$ to $\rho = R = 4.27a_\rho$. The distance between the two fronts at $t = 0$, in units of a_ρ , is $2\pi/k$.

The same scaling is found for $k \rightarrow \infty$ when, since \tilde{v} is vanishingly small at all times, Eq. (18) reduces to an equation for the amplitude \tilde{u} only: $i\hbar b^2(t)\partial_t\tilde{u} = [\tilde{H}_\rho + \hbar^2 k^2/(2m)]\tilde{u}$. If \tilde{u} at $t = 0$ is an eigenfunction u_{nk} of $[\tilde{H}_\rho + \hbar^2 k^2/(2m)]$, then it scales as $\tilde{u}(\rho, t) = \exp[-i\omega_{nk}\tau(t)]u_{nk}(\rho)$, as before.

In the general case of a finite and nonzero value of k , the radial and axial degrees of freedom in Eq. (18) are coupled and the functions $|\tilde{u}(\rho)|$ and $|\tilde{v}(\rho)|$ are no more stationary. However, as one can see in Figs. 7 and 8, their time evolution is very slow, at least for the Bogoliubov modes with few radial nodes or none, and the positions of maxima and minima are

almost constant. This is particularly evident for the minimum of $|\tilde{u}|$ in Fig. 8, which remains always very close to the position of the radial node at $t = 0$ (solid circle on the axis).

E. Axial motion: Thomas-Fermi approximation and local wavefront velocity

Here we concentrate on the axial motion of quasiparticles. We first observe that when $\eta \gg 1$ the ground state density of the infinite cylinder is well reproduced by the Thomas-Fermi approximation $gn_0(\rho) = \mu_{\text{TF}} - V(\rho)$, which corresponds to neglecting the quantum pressure $-\hbar^2/(2m)\nabla_\rho^2$ in the stationary GP equation (4). This also implies that $g\tilde{n}_0(\rho) = \mu_{\text{TF}} - V(\rho)$ during the expansion. We also notice that the amplitudes \tilde{u} and \tilde{v} of axial phonons with a small number of radial nodes are smooth functions of ρ at all times. This means that the term $[\hbar^2/(2m)]\nabla_\rho^2$ can safely be neglected also in Eq. (18), if we are not interested in the details of the radial motion. With these approximations, expression (8) gives $\tilde{H}_\rho = g\tilde{n}_0$ and Eq. (18) becomes

$$i\hbar\partial_t \begin{pmatrix} \tilde{u} \\ \tilde{v} \end{pmatrix} = H(t) \begin{pmatrix} \tilde{u} \\ \tilde{v} \end{pmatrix} \quad (23)$$

where

$$H(t) = \frac{g\tilde{n}_0}{b^2(t)} \begin{pmatrix} 1 & 1 \\ -1 & -1 \end{pmatrix} + \frac{\hbar^2 k^2}{2m} \begin{pmatrix} 1 & 0 \\ 0 & -1 \end{pmatrix}. \quad (24)$$

The same equation can be written for the quantities $\tilde{u} + \tilde{v}$ and $\tilde{u} - \tilde{v}$ [33]:

$$i\hbar\partial_t(\tilde{u} + \tilde{v}) = \frac{\hbar^2 k^2}{2m}(\tilde{u} - \tilde{v}) \quad (25)$$

$$i\hbar\partial_t(\tilde{u} - \tilde{v}) = \left(\frac{2g\tilde{n}_0}{b^2(t)} + \frac{\hbar^2 k^2}{2m} \right)(\tilde{u} + \tilde{v}). \quad (26)$$

These equations can be easily decoupled to get the equation of motion for $\tilde{u} + \tilde{v}$:

$$\partial_t^2(\tilde{u} + \tilde{v}) = -\Omega^2(t)(\tilde{u} + \tilde{v}) \quad (27)$$

with

$$\Omega^2(t) = \frac{k^2}{2m} \left(\frac{2g\tilde{n}_0}{b^2(t)} + \frac{\hbar^2 k^2}{2m} \right). \quad (28)$$

The quantity Ω is the frequency of Bogoliubov excitations in a uniform gas having time-dependent density $\tilde{n}_0/b^2(t)$. Recalling definition (20), one can identify the quantity

$$\tilde{c} = \frac{\Omega}{k} = \left[\frac{g\tilde{n}_0}{mb^2(t)} + \left(\frac{\hbar k}{2m} \right)^2 \right]^{1/2}. \quad (29)$$

with the axial phase velocity of density modulations associated with the expanding phonons. This velocity depends on ρ through $\tilde{n}_0(\rho)$. One can insert the Thomas-Fermi density profile of the infinite cylinder and the expression of $b(t)$ to get

analytic results for the wavefront position vs. time. Typical results of this local density approximation are shown in Fig. 11 and can be compared with those obtained from the numerical integration of the rescaled Bogoliubov equations, in Fig. 10. There is a good qualitative agreement both at low and high k , even though, as expected, the local density approximation overestimates the ρ -dependence of \tilde{c} , especially for the motion near the surface of the condensate, where Thomas-Fermi approximation fails.

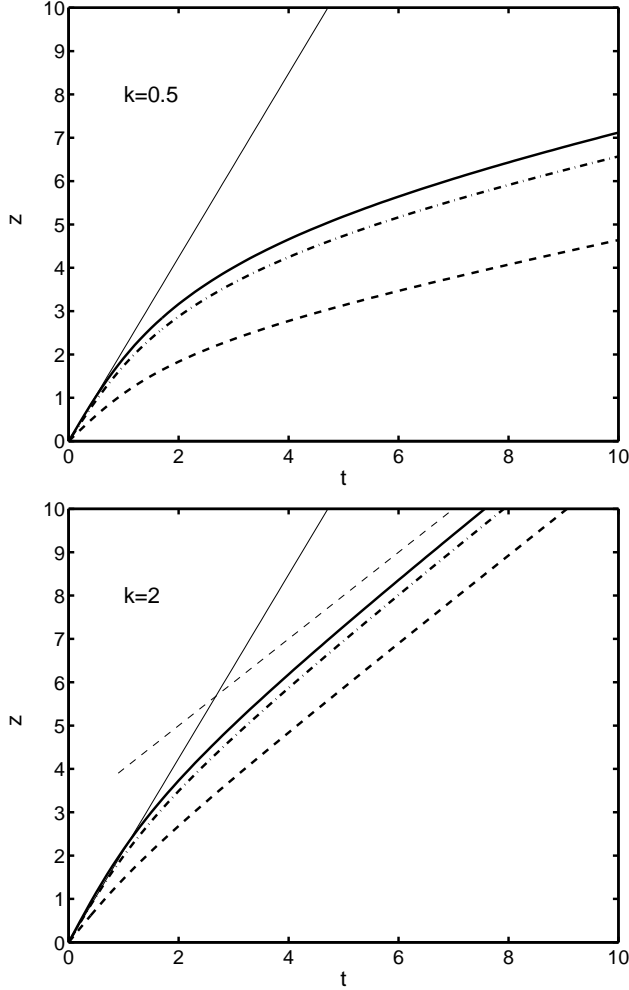


FIG. 11: Same as in Fig. 10, but using the local velocity (29) to get the wavefront position at each ρ and t .

IV. ADIABATIC QUASIPARTICLE-TO-PARTICLE EVAPORATION

In Eqs. (23)-(24) the quantities \tilde{n}_0 , \tilde{u} and \tilde{v} depend on ρ , but one can extract useful results also by averaging out this weak ρ -dependence. A simple approach consists of taking a constant rescaled density \tilde{n}_0 equal to the radial average $\langle \tilde{n}_0(\rho) \rangle_\rho = \tilde{n}_0(0)/2$. Then, one can choose the initial \tilde{u} and \tilde{v} as the ρ -independent quasiparticle amplitudes of phonons in a uniform gas of that density and for a given k . Finally, one

can solve Eq. (23) for the time evolution of the rescaled amplitudes. The resulting behavior of the function $|\tilde{v}(t)|^2$, normalized to its value at $t = 0$, is shown in Fig. 9 for different k (dashed lines). The remarkable agreement with the results for $\langle |\tilde{v}|^2 \rangle$ obtained from the rescaled Bogoliubov equations (18) tells us that the evolution of a quasiparticle in the inhomogeneous cylindrical condensate is very similar to the one in a uniform gas having a density that decreases in time as $b^{-2}(t) = (1 + \omega_\rho^2 t^2)^{-1}$.

An interesting reformulation of the same problem is found by considering Eq. (23) as the evolution of a two level system governed by a nonhermitian time-dependent Hamiltonian. Let us rewrite Eq. (23) in the form

$$i\hbar\partial_t|\delta\tilde{\Psi}\rangle = H(t)|\delta\tilde{\Psi}\rangle \quad (30)$$

with

$$|\delta\tilde{\Psi}\rangle = \begin{pmatrix} \tilde{u} \\ \tilde{v} \end{pmatrix}. \quad (31)$$

Then let us recall definition (28) and introduce the quantity $\Theta(t)$ such that $\hbar\Omega \sinh \Theta = g\tilde{n}_0/b^2(t)$ and $\hbar\Omega \cosh \Theta = g\tilde{n}_0/b^2(t) + \hbar^2 k^2/(2m)$. Thus

$$\tanh\Theta(t) = g\tilde{n}_0 \left(g\tilde{n}_0 + \frac{\hbar^2 k^2}{2m} b^2(t) \right)^{-1} \quad (32)$$

and Hamiltonian (24) can be rewritten as

$$H(t) = \hbar\Omega(t) \begin{pmatrix} \cosh \Theta(t) & \sinh \Theta(t) \\ -\sinh \Theta(t) & -\cosh \Theta(t) \end{pmatrix}. \quad (33)$$

This Hamiltonian is nonhermitian. At any given time t , it admits two real eigenvalues $\pm\Omega$ and the corresponding biorthonormal set of eigenvectors $\{|\pm\rangle_r, |\pm\rangle_l\}$, where the "right" and "left" eigenvectors are defined by

$$H(t)|\pm\rangle_r = \pm\hbar\Omega(t)|\pm\rangle_r \quad (34)$$

$$H^\dagger(t)|\pm\rangle_l = \pm\hbar\Omega(t)|\pm\rangle_l. \quad (35)$$

A simple calculation yields

$$|+\rangle_r = \frac{1}{\sqrt{2}} \begin{pmatrix} \sqrt{\cosh \Theta + 1} \\ -\sqrt{\cosh \Theta - 1} \end{pmatrix} \quad (36)$$

$$|-\rangle_r = \frac{1}{\sqrt{2}} \begin{pmatrix} -\sqrt{\cosh \Theta - 1} \\ \sqrt{\cosh \Theta + 1} \end{pmatrix} \quad (37)$$

$${}_l\langle +| = \frac{1}{\sqrt{2}} (\sqrt{\cosh \Theta + 1}, \sqrt{\cosh \Theta - 1}) \quad (38)$$

$${}_l\langle -| = \frac{1}{\sqrt{2}} (\sqrt{\cosh \Theta - 1}, \sqrt{\cosh \Theta + 1}). \quad (39)$$

These vectors obey the orthogonality relations

$${}_l\langle +|+\rangle_r = {}_l\langle -|-\rangle_r = 1 \quad (40)$$

$${}_l\langle +|-\rangle_r = {}_l\langle -|+\rangle_r = 0. \quad (41)$$

They also satisfy the relations

$${}_l\langle \pm|\partial_t|\pm\rangle_r = 0 \quad (42)$$

$${}_l\langle \mp|\partial_t|\pm\rangle_r = -(1/2)\partial_t\Theta(t) \quad (43)$$

with

$$\partial_t \Theta(t) = -\frac{\partial_t b^2(t)}{b^2(t)} \frac{g\tilde{n}_0}{2g\tilde{n}_0 + \hbar^2 k^2 b^2(t)/(2m)}. \quad (44)$$

Notice that the \tilde{u} and \tilde{v} components of the eigenvectors (36)-(39) are such that $|\tilde{u}|^2 - |\tilde{v}|^2 = \pm 1$ for $|\pm\rangle$ states, with eigenfrequency $\pm\Omega$. At $t = 0$ the state $|+\rangle_r$, corresponds to a quasiparticle of wavevector k and frequency $\Omega(0) = \{k^2/(2m)[2g\tilde{n}_0 + \hbar^2 k^2/(2m)]\}^{1/2}$, whose components, $\tilde{u} = u_k$ and $\tilde{v} = v_k$, are the usual amplitudes of a Bogoliubov mode in a uniform gas. At $t \rightarrow \infty$ the same state corresponds to a free atom with the same k and frequency $\Omega(\infty) = \hbar k^2/(2m)$. The time evolution of the state $|+\rangle_r$ is simply obtained by using the expression (36) and the definitions of $\Theta(t)$ and $\Omega(t)$. For example, one gets

$$\tilde{v}^2(t) = \frac{g\tilde{n}_0/b^2(t) + \hbar^2 k^2/(2m)}{2\hbar\Omega(t)} - \frac{1}{2}, \quad (45)$$

which has the two correct limits $\tilde{v}^2(0) = v_k^2 = [g\tilde{n}_0 + \hbar^2 k^2/(2m)]/(2\hbar\Omega(0)) - 1/2$ [34] and $\tilde{v}^2(\infty) = 0$. In the large k limit, when $\hbar^2 k^2/(2m) \gg g\tilde{n}_0$, Eq. (45) gives

$$\tilde{v}(t) = \frac{mg\tilde{n}_0}{\hbar^2 k^2 b^2(t)}. \quad (46)$$

Now, let us use the basis of instantaneous eigenvectors $\{|\pm\rangle_r\}$ to project the state $|\delta\Psi\rangle$ as

$$|\delta\Psi\rangle = c_+|+\rangle_r + c_-|-\rangle_r \quad (47)$$

and assume that the initial state is just a quasiparticle of momentum $\hbar k$, that is $c_+ = 1$ and $c_- = 0$ at $t = 0$. The evolution of $|\delta\Psi\rangle$ is governed by the Schrödinger equation (30). By using the new basis together with the properties (40)-(44), the same equation can be rewritten in the form

$$i\partial_t \begin{pmatrix} c_+(t) \\ c_-(t) \end{pmatrix} = \begin{pmatrix} \Omega(t) & \frac{i}{2}\partial_t\Theta(t) \\ \frac{i}{2}\partial_t\Theta(t) & -\Omega(t) \end{pmatrix} \begin{pmatrix} c_+(t) \\ c_-(t) \end{pmatrix}. \quad (48)$$

The numerical integration of this equation gives, of course, the same results of Eq. (30) (dashed lines for $|\tilde{v}|^2$ in Fig. 9, for instance), but the use of a different basis makes the evaporation mechanism more transparent. In fact, it allows one to point out the interesting situation that occurs when $|\delta\Psi\rangle$ remains close to $|+\rangle_r$ at all times. This *adiabatic following* happens when the diabatic coupling between the two eigenstates is small, i.e., when the off-diagonal term $|\partial_t\Theta|$ is much smaller than the frequency splitting 2Ω [35]. Now, the function $|\partial_t\Theta(t)|$ vanishes at $t = 0$ and $t \rightarrow \infty$ and is always smaller than $\partial_t b^2/(2b^2)$ which has maximum value $\omega_\rho/2$ for $t = \omega_\rho^{-1}$. Conversely, the function $\Omega(t)$ decreases monotonically from $\Omega(0)$ to $\hbar k^2/(2m)$. Thus the evolution is certainly adiabatic if $\hbar k^2/(2m) \gg \omega_\rho/2$, that means $k \gg a_\rho^{-1}$. This condition is somewhat too restrictive. In fact, the two functions $|\partial_t\Theta|$ and 2Ω might be comparable only around $t = \omega_\rho^{-1}$ and the adiabatic evolution is ensured if $\Omega \gg \omega_\rho$ at that time. Now, for k of the order of a_ρ^{-1} and $\eta = g\tilde{n}_0/(\hbar\omega_\rho) \gg 1$,

the term $g\tilde{n}_0$ in Ω is larger than $\hbar^2 k^2/(2m)$ at $t = 0$, but it remains larger also at $t = \omega_\rho^{-1}$, when $b^2 = 2$. The condition for adiabaticity thus becomes $k \gg \eta^{-1/2} a_\rho^{-1}$. In our case $\eta = 9.1$ and the condition is $k \gg 0.3 a_\rho^{-1}$.

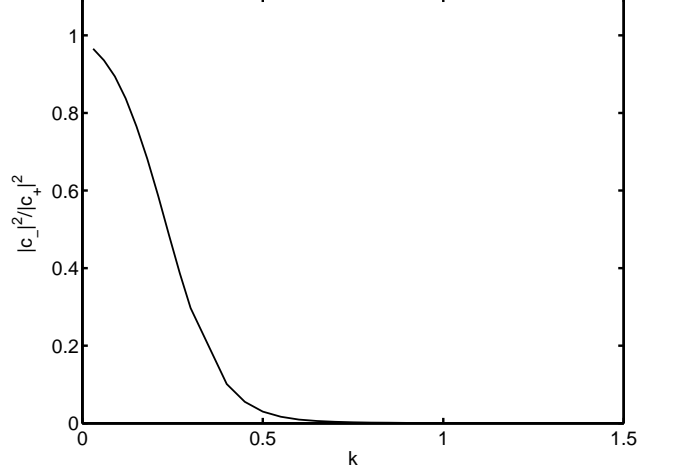


FIG. 12: Ratio $|c_-|^2/|c_+|^2$ at $t \rightarrow \infty$ obtained by solving Eq. (48) for different values of k , in units of a_ρ^{-1} , with the condition $c_+ = 1$ and $c_- = 0$ at $t = 0$.

One can check whether the quasiparticle-to-particle conversion is adiabatic or diabatic by directly comparing the evolution of the state $|\delta\Psi\rangle$ with that of the instantaneous eigenstate $|+\rangle_r$. The difference is a measure of non-adiabaticity. For the quantity \tilde{v}^2 in Fig. 9 the comparison has to be done between dashed lines, that come from the evolution of $|\delta\Psi\rangle$ through Eq. (48), and dot-dashed lines, that come from the evolution of $|+\rangle_r$ through Eq. (45). As one can see, for $k \gg 0.3 a_\rho^{-1}$ the adiabatic following approximation is indeed an accurate description of the evaporation process. The dashed and dot-dashed curves are already indistinguishable for $k = 2 a_\rho^{-1}$ and, for larger k , all curves collapse on the dotted curve, which represents the asymptotic law (46). For low k , conversely, the diabatic coupling between the $|+\rangle_r$ and $|-\rangle_r$ eigenstates, originating from the time-dependence of the scaling parameter $b(t)$, is no more negligible and the state $|\delta\Psi\rangle$ significantly differs from $|+\rangle_r$ both at short and long times. A nice view of this coupling can be seen in Fig. 12, where we plot the value of $|c_-|^2/|c_+|^2$ at $t \rightarrow \infty$ as a function of k . In the adiabatic case this ratio vanishes. At low k , conversely, it tends to 1. From the definitions (36)-(37), one can easily see that the quantity $|c_-|^2/|c_+|^2$ at $t = \infty$ is equal to $|\tilde{v}|^2/|\tilde{u}|^2$ and corresponds to the ratio between the number of atoms moving with opposite momenta $\pm\hbar k$ at $t \rightarrow \infty$, as a result of the evaporation of an initial quasiparticle with momentum $+\hbar k$. It should not be confused, vice-versa, with the ratio $|v_k|^2/|u_k|^2$ at $t = 0$, which is different and is related to $\pm k$ components the momentum distribution of the initial in-trap quasiparticle [3, 8].

V. GP SIMULATIONS REVISITED

We are now ready to use the results of sections III and IV to interpret some relevant features of GP simulations in elongated condensates.

Axial motion of wavefronts

Differently from the infinite cylinder, the elongated condensate expands also in the z -direction. Let us consider Eq. (29) and apply a local density approximation in this form:

$$\tilde{c}(\rho, z, t) = \frac{\dot{b}_z(t)}{b_z(t)} z + \left[\frac{g\tilde{n}_0(\rho, z)}{mb_\rho^2(t)b_z(t)} + \left(\frac{\hbar k}{2mb_z(t)} \right)^2 \right]^{1/2}. \quad (49)$$

The slow expansion along z is here included through the scaling parameter b_z . The new scaling laws are [28, 29, 36]

$$\ddot{b}_\rho(t) = \frac{\omega_\rho^2}{b_\rho^3(t)b_z(t)} ; \quad \ddot{b}_z(t) = \frac{\lambda^2\omega_\rho^2}{b_\rho^2(t)b_z^2(t)}. \quad (50)$$

Thus the first term in \tilde{c} is the local drift velocity due to the axial motion of the “background” in which the excitations move. The second term is now ρ - and z -dependent through the rescaled density $\tilde{n}_0(\rho, z)$. This simple model allows us to plot the wavefront position and speed for the elongated condensate, by using the unperturbed GP density profile at $t = 0$ as input and solving the two coupled equations for b_z and b_ρ . The position of the wavefronts, corresponding to the simulation in Fig. 3, are shown as dashed lines in the same figure. In practice, we take the crests of δn at $t = 0$ from the GP simulation and let them move with velocity \tilde{c} during the expansion for $t > 0$. The dashed lines are the same crests at $t = 25\omega_\rho^{-1}$. They nicely agree with the results of GP simulations (solid lines), except near the surface where the Thomas-Fermi approximation is inadequate.

One can also estimate the position in time of the crests of the linear density (upper part of Fig 3). A simple way consists in propagating each front with a radially averaged velocity, which is obtained by replacing $\tilde{n}_0(\rho, z)$ in Eq. (49) with the average $\langle \tilde{n}_0(\rho, z) \rangle_\rho$. The results are shown as solid lines in Fig. 13, where they are compared with the ones of the GP simulation (empty circles). The thin dashed lines represents the Thomas-Fermi axial size of the expanding condensate. The condensate has maximum density at $z = 0$. All crests move initially with almost the same positive velocity along z . Within a short time interval, when the mean-field is still active, those crests that move downhill (positive z) tend to be accelerated by the expanding background, with respect to their motion in an infinite cylinder. Those that move uphill (negative z) seem to be decelerated, and they can also invert their motion. The agreement with the full GP simulation is remarkable. This means that Eq. (49) accounts for most of the physics involved in the axial motion of density modulations in the expansion of low k phonons.

Threshold for the appearance of a released-phonon cloud

Looking at Figs. 10 and 13 one understands why at low k the excited atoms do not form a separate cloud: they have not

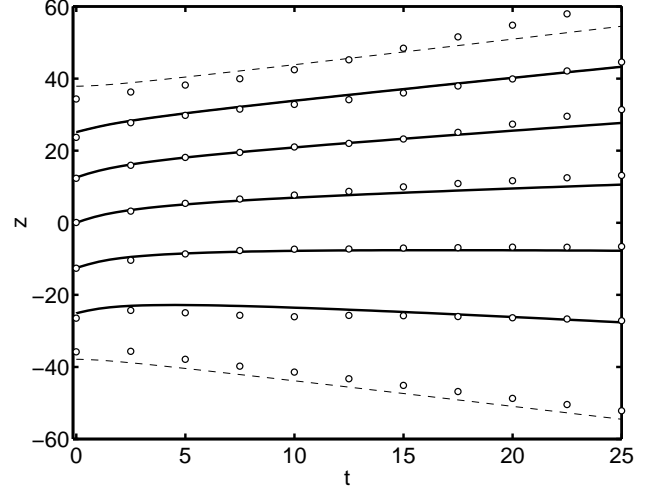


FIG. 13: Wavefront position vs. time for the elongated condensate of Figs. 1 and 3. Points correspond to the crests of the linear density obtained from the GP simulation. Solid lines are the results of the local density model, with local phase velocity given by (49). Thin dashed lines represent the axial size of the expanding condensate. Length and time are in units of a_ρ and ω_ρ^{-1} , respectively.

enough speed to reach the expanding boundary along z . In classical fluids this situation corresponds to the case of sound waves propagating on a background hydrodynamic flow. A boundary that moves faster than the speed of sound acts as an event horizon in a sonic black hole [37]. A possible realization of a stable black hole for long wavelength phonons in ring-shaped Bose-Einstein condensates has been recently proposed in Ref. [38]. Our configuration is nonstationary and the excitations are sound-like waves only at the very beginning of the expansion, in a time interval of the order of ω_ρ^{-1} , when they are still well inside the condensate. Then, the wavefronts reach an almost constant phase velocity, of the order of $\hbar k/(2m)$ and the whole wave packet moves at group velocity $\sim \hbar k/m$. Thus, if the latter is smaller than the velocity of the boundary (upper dashed line in Fig. 13), most of the atoms remain within the expanding condensate at all times. In the limit $\lambda \ll 1$, Eqs. (50) yield the expression $(\pi/2)\omega_\rho\lambda^2 Z_{\text{TF}}$ for the asymptotic velocity of the boundary, where Z_{TF} is its initial position in Thomas-Fermi approximation [29]. Thus the condition for the atoms to exit is $\hbar k/m > (\pi/2)\omega_\rho\lambda^2 Z_{\text{TF}}$. Since $(1/2)m\lambda^2\omega_\rho^2 Z_{\text{TF}}^2 = \mu_{\text{TF}}$ and $\eta = \mu_{\text{TF}}/(\hbar\omega_\rho)$, the same condition can be rewritten as $ka_\rho > \pi\lambda(\eta/2)^{1/2}$. With the parameters of the condensate in section II, this threshold is around $k \sim 0.76a_\rho^{-1}$, in agreement with the transition from the low k scenario of Fig. 1 to the high k scenario of Fig. 2. The transition is not sharp, however, since the excited atoms can reach the boundary at different times and with different velocities so that, for a given expansion time, one can observe a released-phonon cloud only partially separated from the condensate.

Adiabatic and diabatic evaporation

For the elongated condensate of the simulations in section

If one has $\eta^{-1/2} < \pi\lambda(\eta/2)^{1/2} < \eta^{1/2}$. The first value is the threshold for the adiabatic quasiparticle-to-particle evaporation discussed in section IV (see Fig. 12). The second is the threshold for the appearance of a separate released-phonon cloud. The third is the inverse of the healing length. This implies that when the initial excitations are single-particle modes, i.e., with $ka_\rho > \eta^{1/2}$, the excited atoms always move out of the condensate. Instead, when the initial excitations are phonon-like modes, i.e., with $ka_\rho < \eta^{1/2}$, they can either move out or remain inside. However, if they move out as a separate cloud, the evaporation is certainly adiabatic. This means that a single quasiparticle of positive momentum $\hbar k$ gives rise to a single atom moving with the same positive momentum, even though the initial quasiparticle state is made of correlated $+k$ and $-k$ components in the momentum distribution of the atoms. It is worth noticing that, with appropriate choices of λ and η , such that $\pi\lambda(\eta/2)^{1/2} < \eta^{-1/2}$, one can have diabatic evaporation together with the appearance of released-phonon clouds. In this case, one expects to have atoms moving with both positive and negative momentum $\pm\hbar k$ out of the condensate.

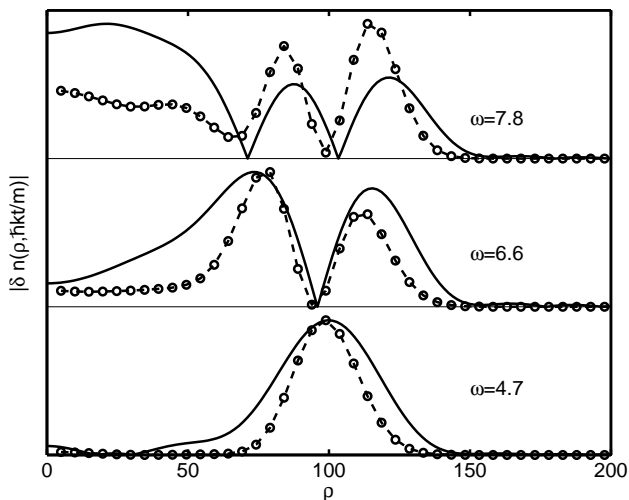


FIG. 14: Radial density profiles, in arbitrary units, of the released-phonon cloud at $z = \hbar kt/m$, with $t = 25\omega_\rho^{-1}$, $k = 2.5a_\rho^{-1}$ and three different values of ω . Points with dashed lines are the results of GP simulations with $V_B = 0.3\hbar\omega_\rho$ and $t_B = 4\omega_\rho^{-1}$. Solid lines are the functions $|u_{nk} + v_{nk}|$ for an infinite cylinder with $\eta = 9.1$, the same k and $n = 0$ (bottom), 1 (mid) and 2 (top).

Radial scaling of nodal lines

In section II, we have seen that the released-phonon cloud exhibits a “shell” structure (see Figs. 2 and 4). It can be reasonably assumed that the scaling of the radial motion, which is almost exact for the infinite cylinder, is still valid also for the elongated condensate. This means that an excited state having a radial node at a point $\rho_0(z)$ at $t = 0$ should produce a cloud of excited atoms having a minimum of density close

to $\rho_0/b(t)$, but translated along z as a consequence of the axial motion. If this is true, the shell structure in Figs. 2 and 4 is an indication that, even though we used a Bragg frequency in resonance with the lowest phonon branch with no nodes, some quasiparticles in the next branches, with one and two radial nodes, were also excited. In order to be more selective, one has to use Bragg pulses with longer duration t_B [11, 12]. We thus repeat the same type of simulations of Figs. 2 and 4, for $k = 2.5a_\rho^{-1}$, but with $t_B = 4\omega_\rho^{-1}$. The Bragg frequency is varied in such a way to excite phonons with 0, 1 and 2 radial nodes. We find a significant change in the shell structure of the released-phonon cloud. In Fig. 14 we plot a cut of its density distribution at $z = \hbar kt/m$, with $t = 25\omega_\rho^{-1}$, which corresponds roughly to the position where the moving cloud has its maximum radial extension. The three density profiles obtained from GP simulations (points with dashed lines) are compared with the shape of the functions $|u_{nk} + v_{nk}|$ (solid lines), calculated at $\rho/b(t)$, for the Bogoliubov modes of an infinite cylinder, with the same k and with $n = 0, 1$ and 2. The good agreement confirms that the nodal lines scale almost exactly and that the observation of radial structures in the released-phonon cloud can be an efficient tool for the identification of the initial in-trap quasiparticles.

VI. CONCLUSIONS

We have shown that the evaporation of phonons in a freely expanding condensate is an interesting quantum process with a rich variety of scenarios. Our analysis is based on the GP theory at zero temperature and in the linear response regime, where the concept of quasiparticle is well defined. We have thus neglected possible effects of thermal and quantum fluctuations, as well as those of nonlinear dynamics. This is justified if one assumes that the population of the initially excited phonon-like mode is large enough to neglect fluctuations and small enough to remain in the linear regime. For condensates with 10^5 to 10^6 atoms or more, this condition is ensured by choosing the Bragg intensity and duration such to excite about 1 to 10% of the atoms as in typical experiment. In this paper, we have provided explicit calculations for an elongated condensate similar to that of current experiments, but the results obtained for the infinite cylinder are rather general. The extension of this analysis to different sets of parameters can lead to different regimes that are also worth exploring.

Acknowledgments

We are indebted to N. Davidson, N. Katz, R. Ozeri, L. Pitaevskii, P.O. Fedichev, P. Massignan, M. Modugno and L. Ricci for useful discussion. This work is supported by the Ministero dell’Istruzione, dell’Università e della Ricerca. One of the authors (FD) thanks the Dipartimento di Fisica di Trento for the hospitality.

-
- [1] N. N. Bogoliubov, J. Phys. (USSR) **11**, 23 (1947).
- [2] D. M. Stamper-Kurn, A. P. Chikkatur, A. Görlitz, S. Inouye, S. Gupta, D. E. Pritchard, and W. Ketterle, Phys. Rev. Lett. **83**, 2876 (1999).
- [3] J. M. Vogels, J. M. Vogels, K. Xu, C. Raman, J. R. Abo-Shaer, and W. Ketterle, Phys. Rev. Lett. **88**, 060402 (2002).
- [4] J. Steinhauer, R. Ozeri, N. Katz, and N. Davidson Phys. Rev. Lett. **88**, 120407 (2002).
- [5] R. Ozeri, J. Steinhauer, N. Katz, and N. Davidson, Phys. Rev. Lett. **88**, 220401 (2002).
- [6] N. Katz, J. Steinhauer, R. Ozeri, and N. Davidson, Phys. Rev. Lett. **89**, 220401 (2002).
- [7] F. Zambelli, L. Pitaevskii, D.M. Stamper-Kurn, and S. Stringari, Phys. Rev. A **61**, 063608 (2000).
- [8] A. Brunello, F. Dalfovo, L. Pitaevskii, and S. Stringari, Phys. Rev. Lett. **85**, 4422 (2000); A. Brunello, F. Dalfovo, L. Pitaevskii, S. Stringari, and F. Zambelli, Phys. Rev. A **64**, 063614 (2001).
- [9] E. Gershnabel, N. Katz, R. Ozeri, E. Rowen, J. Steinhauer, N. Davidson, e-print cond-mat/0309584.
- [10] F. Dalfovo, S. Giorgini, L. Pitaevskii and S. Stringari, Rev. Mod. Phys. **71**, 463 (1999).
- [11] J. Steinhauer, N.Katz, R. Ozeri, N. Davidson, C. Tozzo, and F. Dalfovo, Phys. Rev. Lett. **90**, 060404 (2003).
- [12] C. Tozzo and F. Dalfovo, New J. Phys. **5**, 54 (2003).
- [13] M. Brown and A.F.G. Wyatt, J. Phys.: Condens. Matter **2**, 5025 (1990).
- [14] J.C. Garrison and E.M. Wright, Phys. Lett. A **128**, 177 (1988); M. Gorlicki, Phys. Rev. A **49**, 4339 (1994).
- [15] S. Dettmer, D. Hellweg, P. Ryytty, J.J. Arlt, W. Ertmer, K. Sengstock, D.S. Petrov, G.V. Shlyapnikov, H. Kreutzmann, L. Santos, and M. Lewenstein, Phys. Rev. Lett. **87**, 160406 (2001).
- [16] P.O. Fedichev and U.R. Fisher, e-print cond-mat/0304342 and cond-mat/0307200.
- [17] L.P. Pitaevskii, Zh. Eksp. Teor. Fiz. **40**, 646 (1961) [Sov. Phys. JETP **13**, 451 (1961)]; E.P. Gross, Nuovo Cimento **20**, 454 (1961).
- [18] F. Dalfovo and S. Stringari, Phys. Rev. A **53**, 2477, (1996).
- [19] P.B. Blakie and R.J. Ballagh, J. Phys. B **33**, 3961 (2000); P.B. Blakie, R.J. Ballagh, and C.W. Gardiner, Phys. Rev. A **65**, 033602 (2002).
- [20] M. Modugno, L. Pricoupenko, and Y. Castin, Eur. Phys. J. D **22**, 235 (2003).
- [21] P. Massignan and M. Modugno, Phys. Rev. A **67**, 023614 (2003).
- [22] E. Zaremba, Phys. Rev. A **57**, 518 (1998); S. Stringari, Phys. Rev. A **58**, 2385 (1998)
- [23] N. Davidson, N. Katz and R. Ozeri, private communication.
- [24] P.O. Fedichev and G.V. Shlyapnikov, Phys. Rev. A **63**, 045601 (2001).
- [25] M. Guilleumas and L. Pitaevskii, Phys. Rev. A **67**, 053607 (2003).
- [26] S. Komineas and N. Papanicolaou, Phys. Rev. A **67**, 023615 (2003).
- [27] F. Dalfovo, S. Giorgini, M. Guilleumas, L.Pitaevskii and S. Stringari, Phys. Rev. A **56**, 3840 (1997).
- [28] Y. Kagan, E.L. Surkov and G.V. Shlyapnikov, Phys. Rev. A **54**, R1753 (1996); Phys. Rev. A **55**, R18 (1997).
- [29] Y. Castin and R. Dum, Phys. Rev. Lett. **77**, 5315 (1996).
- [30] L.P. Pitaevskii and A. Rosch, Phys. Rev. A **55**, R853 (1997).
- [31] S. Stringari, Phys. Rev. Lett. **77**, 2360 (1996).
- [32] F.Dalfovo and M.Modugno, Phys. Rev. A **61**, 023605 (2000).
- [33] Yu. Kagan and L.A. Maksimov, Phys. Rev. A **64**, 053610 (2001). In this paper a similar approach was used to predict the coupling between axial phonons and radial breathing oscillations.
- [34] L. Pitaevskii and S. Stringari, *Bose-Einstein Condensation*, (Oxford University Press, Oxford, 2003) p.31.
- [35] A. Messiah, *Quantum Mechanics* (North-Holland, Amsterdam, 1961), Chap. XVII-13.
- [36] F. Dalfovo, C. Minniti, S. Stringari, and L. Pitaevskii, Phys. Lett. A **227**, 259 (1997); F. Dalfovo, C. Minniti and L.P. Pitaevskii, Phys. Rev. A **56**, 4855 (1997); F. Dalfovo, Proceedings of the Int. School E. Fermi, Course CXL, Varenna (IOS Press, Amsterdam, 1999) p. 555.
- [37] W.G. Unruh, Phys. Rev. Lett. **46**, 1352 (1981), and Phys. Rev. D **51**, 2827 (1995); M. Visser, Phys. Rev. Lett. **80**, 3436 (1998), and Class. Quantum Grav. **15**, 1767 (1998).
- [38] L.J. Garay, J.R. Anglin, J.I. Cirac, and P. Zoller, Phys. Rev. Lett. **85**, 4643 (2000), and Phys. Rev. A, **63**, 023611 (2001)